Biochar from raw and spent common ivy: Impact of preprocessing and pyrolysis temperature on biochar properties

Non Peer-reviewed author version

VERCRUYSSE, Willem; Smeets, Jolien; HAELDERMANS, Tom; JOOS, Bjorn; HARDY, An; SAMYN, Pieter; YPERMAN, Jan; VANREPPELEN, Kenny; CARLEER, Robert; ADRIAENSENS, Peter; MARCHAL, Wouter & VANDAMME, Dries (2021)
Biochar from raw and spent common ivy: Impact of preprocessing and pyrolysis temperature on biochar properties. In: Journal of analytical and applied pyrolysis (Print), 159 (Art N° 105294).

DOI: 10.1016/j.jaap.2021.105294
Handle: http://hdl.handle.net/1942/34706

Biochar from raw and spent common ivy: impact of preprocessing and pyrolysis temperature on biochar properties

Willem Vercruysse (Conceptualization) (Data curation) (Funding acquisition) (Investigation) (Methodology) (Project administration) (Writing - original draft), Jolien Smeets (Investigation), Tom Haeldermans (Investigation) (Writing - review and editing), Bjorn Joos (Investigation) (Writing - review and editing), An Hardy (Investigation) (Writing - review and editing), Pieter Samyn (Investigation) (Writing - review and editing), Jan Yperman (Resources) (Writing - review and editing), Kenny Vanreppelen (Resources) (Writing - review and editing), Robert Carleer (Resources) (Writing - review and editing), Peter Adriaensens (Resources) (Writing - review and editing), Wouter Marchal (Funding acquisition) (Resources) (Methodology) (Supervision) (Writing - review and editing), Dries Vandamme (Funding acquisition) (Methodology) (Resources) (Supervision) (Validation) (Writing - review and editing)

PII: S0165-2370(21)00280-1

DOI: https://doi.org/10.1016/j.jaap.2021.105294

Reference: JAAP 105294

To appear in: *Journal of Analytical and Applied Pyrolysis*

Received Date: 25 May 2021

Revised Date: 9 August 2021

Accepted Date: 10 August 2021

Please cite this article as: Vercruysse W, Smeets J, Haeldermans T, Joos B, Hardy A, Samyn P, Yperman J, Vanreppelen K, Carleer R, Adriaensens P, Marchal W, Vandamme D, Biochar from raw and spent common ivy: impact of preprocessing and pyrolysis temperature on

biochar properties, *Journal of Analytical and Applied Pyrolysis* (2021),
doi: https://doi.org/10.1016/j.jaap.2021.105294

Biochar from raw and spent common ivy: impact of preprocessing and pyrolysis temperature on biochar properties

Authors: Willem Vercruysse[a], Jolien Smeets[a], Tom Haeldermans[a,b], Bjorn Joos[c], An Hardy[C], Pieter Samyn[a], Jan Yperman[a], Kenny Vanreppelen[a,b], Robert Carleer[a], Peter Adriaensens[a], Wouter Marchal[a], Dries Vandamme[a*]

[a]UHasselt - Hasselt University, Analytical and Circular Chemistry, Centre for Environmental Sciences (CMK), Institute for Materials Research (IMO-IMOMEC), Agoralaan, 3590 Diepenbeek, Belgium

[b]Act & Sorb, BV, Geleenlaan 31, Genk, 3600, Belgium

[c]UHasselt - Hasselt University, Materials Chemistry - Design and synthesis of inorganic nanomaterials, Institute for Materials Research (IMO-IMOMEC) and Energyville, Agoralaan, 3590 Diepenbeek, Belgium

*dries.vandamme@uhasselt.be

Graphical abstract

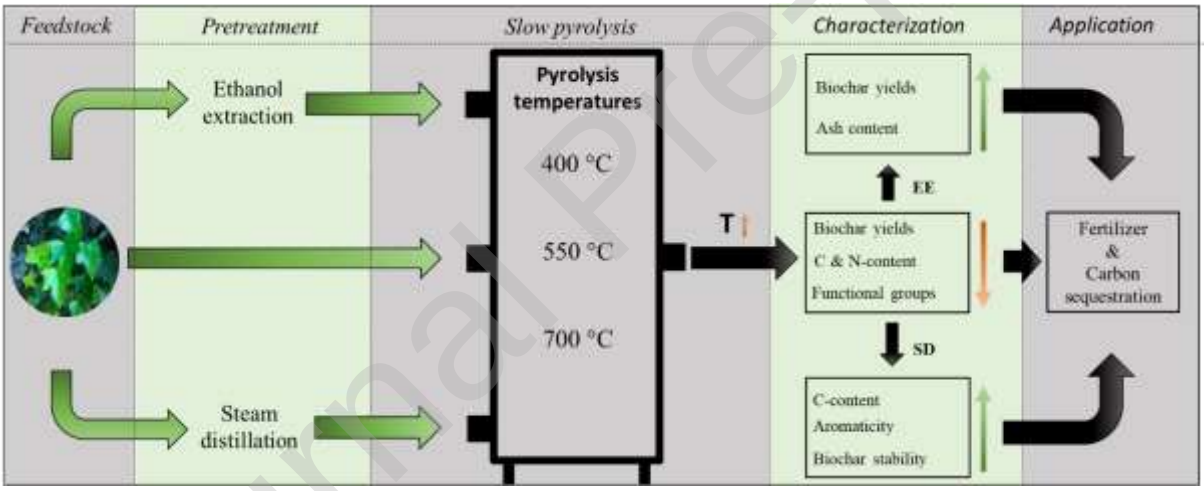

Highlights

- Ivy is a promising biomass feedstock for pyrolysis based biorefinery processes
- A pyrolysis temperature of 400 °C yields high-quality biochars
- Ethanol extractions increase biochar carbon sequestration potential by 20%
- Steam distillations improve biochar's carbon content (12% at 700 °C)

Abstract

Hedera helix L., the common ivy, is an excellent evergreen climbing plant to be applied in vertical green walls to improve urban ecosystems. These green walls need to be trimmed regularly, yielding a biomass stream, which could be promising as a renewable feedstock for biochar production and the extraction of valuable chemicals. The potential of raw and spent (extracted) common ivy as a biochar feedstock was evaluated using slow pyrolysis at different temperatures: 400, 550 and 700 °C. Biochars produced at 400 °C showed a high carbon, nitrogen and ash content, while still having residual surface functionalities. These biochars are therefore interesting to be applied as soil fertilizer. Additionally, it was found that the impact of different green extraction processes (ethanol extraction versus steam distillation) before pyrolysis on the biochar properties was generally positive. Ethanol extractions increased biochar yields and the fraction of inorganic nutrients. Furthermore, ethanol extractions increased the carbon sequestration potential compared to raw ivy. Steam distilled biochar exhibited a very high carbon content (83%), biochar stability (97%) and aromaticity (100%). Steam distillation did not affect the carbon sequestration potential. In conclusion, this investigation affirms common ivy as a promising feedstock for pyrolysis based biorefinery processes.

Keywords: Common ivy, slow pyrolysis, biochar, extraction, pyrolysis temperature

Graphical Abstract

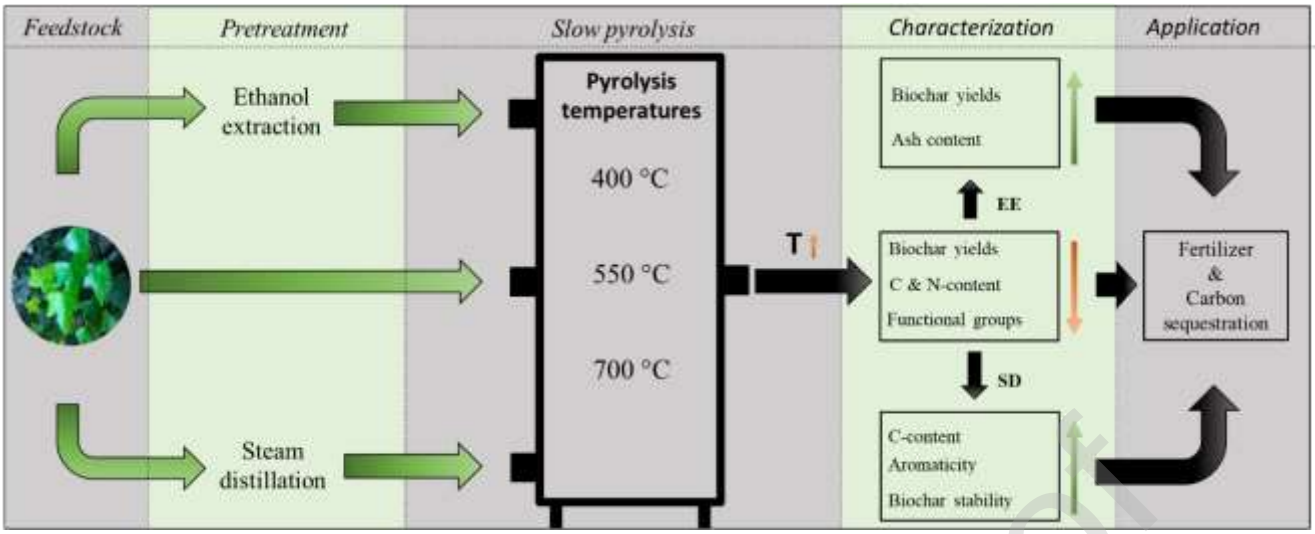

1 Introduction

Urban ecosystems can be improved using common ivy, *Hedera helix L.*, as coverage in green walls, as this contributes to the phytoremediation of polluted air [1] and it decreases urban heat island effects [2]. These green walls will produce an ivy biomass stream, as they need to be trimmed regularly. Therefore, applications for this residual stream should be investigated. Common ivy could be a promising biomass feedstock for a sustainable biorefinery, due to its beneficial properties such as fast growth rate and its ability to be cultivated in vertical systems without the need for large areas of fertile land [3]. Moreover, this plant species contains a lot of interesting extractable compounds, e.g. triterpenoid saponins and volatile oils [4–6], useful as building blocks for pharmaceutical and cosmetic industries [7–9]. The most important triterpenoid saponins for pharmacological applications are hederacoside C (kalopanax saponin B) (2.2 wt% in leaves [10]) and its derivative α-Hederin (0.04 wt% in leaves [10]), furthermore minor quantities of Hederacoside B and D (ratio C:B:D is 1000:75:45) are found. Examples of abundant volatile oils include α-, β-pinene, germacrene D, β-caryophyllene, sabinene, … [7].

These extracts are currently industrially obtained based on following best available technologies. On the one hand, an extraction with ethanol is done to produce hederacoside-rich pharmacological ivy extracts [8,11,12]. A volatile oil extract, on the other hand, of common ivy can be isolated by steam distillation [13,14]. This extraction approach (i.e. steam distillation of biomass) as pretreatment prior to further processing was previously reported for the production of biochars from spent mallee leaves. It improved the nutrient recycling properties of these biochars, i.e. biochar derived from spent biomass had a lower nutrient release in leaching experiments compared to raw biomass derived biochar [15].

The valorization strategy described above incites the idea of a new biorefinery concept that entails the co-production of both ivy extracts coupled with additional value creation by processing the spent (extracted) ivy biomass, which is conventionally discarded. This can be accomplished via slow pyrolysis of the spent ivy biomass, which generates three product streams, of which the solid fraction (biochar) is the most prominent. Liquid- (bio-oil) and gaseous (syngas) products are produced to a lesser extent in slow pyrolysis processes [16]. The produced biochar can be applied by itself or used as a sustainable carbonaceous resource for advanced material design [17]. To the best of our knowledge, no biochar studies using ivy as a feedstock have been published so far, nor has there been any report available on the effect of the proposed extraction approaches on the ivy biochar properties.

The production of biochar is currently mostly studied in the context of its applicability as slow-release soil fertilizer [18]. Biochar, derived from plant material, has several beneficial properties which could improve plant growth after application to soil, such as a large available nutrient content, high pH (to neutralize acidic soils), low amounts of heavy metals as well as some beneficial adsorption properties [19]. Biochar with a high degree of

aromaticity is favorable for carbon sequestration, because of its higher stability in soils [20]. This enhanced stability will subsequently improve biochar's carbon sequestration potential (>50% of carbon is usually retained in soil) [21].

The aim of this study is to investigate the potential of common ivy as a biochar precursor. ~~and to provide insight in the biochar's applicability as soil fertilizer and its carbon sequestration purposes~~. This is done by the characterization of essential properties (elemental composition, thermal degradation behavior, surface functional groups, stability, aromaticity and specific surface area) of the biochars produced from raw ivy. In particular, the biochar production process (i.e. pyrolysis temperature) is optimized depending on these earlier mentioned properties. Finally, the effect of the extraction treatment (ethanol versus steam extraction) on the biochar properties is studied. Effects on biochar yield, surface texture and morphology, elemental composition and ash content are compared with biochar produced from raw ivy.

2 Materials and methods

2.1 Biomass collection

Mixed (leaves and branches) common ivy samples were collected while pruning in spring 2019, in a rural area near Heusden-Zolder, Limburg, Belgium. To ensure sample homogeneity, large sample sizes (>10 kg) were collected. Subsequently, the sample was divided into three batches of approx. 500 g for batch experiments. The first and second batch were dried at 40 °C for 3 days to constant weight. Afterwards both batches were shredded (Retsch SM 100, Haan, Germany) and sieved with mesh size 10 (2 mm). The first untreated batch (raw ivy or RI) was directly pyrolyzed while the second and third batch were used for extraction prior to pyrolysis. The second batch (ethanol extracted ivy or EI) was

subjected to ethanol extraction and afterwards dried to constant weight at 105 °C. The third part (steam distilled ivy or SI) was shredded to 10x10 mm^2 immediately after harvesting to prevent the escape of volatile oils prior to steam distillation. After steam distillation, a dewatering step was carried out after deposition of the SI, followed by drying to constant weight at 105 °C and shredding to an identical size as RI and EI. After shredding, each batch was pyrolyzed, resulting in three different types of biochar: raw ivy biochar (further called RIB), ethanol extracted ivy biochar (EIB) and steam distilled ivy biochar (SIB).

2.2 Biomass pretreatment

The ethanol-extractable fraction was obtained from ivy samples using an optimized ethanol extraction protocol, adapted from ASTM E1690-01 [22]. A Soxhlet extraction was performed for 4 hours using 160 ml ethanol (≥96% (v/v), TechniSolv®, VWR Chemicals) on 20 g dried sample each.

Steam distillations were carried by adding 40 ml of milli-Q water to 60 g of wet shredded sample in the distillation flask. Distillation was performed with a flow rate of approx. 2.5 ml water/min for 60 min and at a temperature of 105 °C. After removal of biomass a condensate fraction was captured, further called steam distillation condensate (SDC).

2.3 Biochar production

Conventional pyrolysis was performed using a home-built stainless steel (AISI 304) batch reactor with a rotating screw [23], [24]. Biomass input was 40 g per pyrolysis experiment. The pyrolysis heating rate was set to 20 °C/min, up to set point temperatures of 400, 550 and 700 °C, under a 70 mL/min nitrogen flow rate. Effective pyrolysis temperature logging is provided and can be found in supplementary data (Figure S1). For the sake of simplicity, set point temperatures will be used to describe the produced biochars. An isothermal period of 30 minutes was maintained after the set point was reached. Temperature was controlled

using a type K thermocouple and adjusted by a FGH 1000 controller driving a Nabertherm R50/250/12 tube furnace. After pyrolysis, the resulting biochar was weighed and yields were determined. Each pyrolysis experiment was repeated in triplicate. Data were reported as mean values (n = 3) with their respective standard errors (1σ). To assess significance of data two tailed student's t-tests, with a confidence interval of 95%, were done after equality of variances was established (F-test).

2.4 Biochar and biomass characterization techniques

2.4.1 Ultimate analysis

A Thermo Electron Flash EA1112 elemental analyzer (ThermoFisher Scientific, Waltham, USA) was used to determine total carbon, hydrogen, nitrogen and sulfur content of all samples. Calibration was performed using BBOT ((2,5-bis (5-tert-butyl-benzoxazol-2-yl) thiophene) (pure, ThermoScientific). Ash content was determined using method ASTM D2866 - 94 [25]. Total oxygen content was calculated by difference (O (wt%) = 100% – C (wt%) – N (wt%) – H (wt%) – S (wt%) – Ash (wt%)). However, no sulfur could be detected in the ivy samples.

2.4.2 Proximate analysis

Proximate analysis was carried out by thermogravimetric analysis (TGA), using a TA instruments Q500 apparatus (TA instruments, New Castle, USA) with the following temperature program: From room temperature to 600 °C, a 20 °C/min heating rate under dynamic nitrogen atmosphere (90 ml/min) was employed, while the atmosphere was switched to oxygen (90 ml/min) and heating was continued, at the same rate, to 900 °C. Sample sizes were 5-10 mg. For both raw ivy, spent ivy and biochar samples volatile matter (Mass loss from 20 °C – 600 °C under N_2-atmosphere) and fixed carbon (mass loss at 600 °C under O_2-atmosphere) were determined.

2.4.3 Surface functional groups using FTIR

Fourier-transform infrared spectroscopy (FTIR) was carried out on all biochar samples using a Vertex 70 Spectrometer equipped with a DTGS detector and attenuated total reflection (ATR) accessory (diamond crystal) (Bruker, Billerica, USA). Biochar absorbance was measured from 4000 – 600 cm^{-1}, with a spectral resolution of 4 cm^{-1}. Baseline correction and normalization at the largest peak (different for each group of samples) were done. Reference spectra of cellulose, hemicellulose and lignin were also measured using α-cellulose (Sigma), xylan from birch wood (Fluka) and lignin, alkali, carboxylated (Aldrich), respectively (supplementary materials, Figure S3). Band assignment was done following several key reference papers ([26], [27], [28], [29], [30], [31], [32], [24]).

2.4.4 Specific surface area using BET

The textural characteristics of the biochars were determined by measuring the N_2 adsorption and desorption isotherms at 77 K using a Tristar II 3020 surface area analyzer (Micromeritics, Norcross, USA). The sample was degassed under nitrogen flow at 150 °C for 16 h prior to measurement in order to remove any residual moisture and other volatile contaminants. The specific surface area (S_{BET}) was estimated using the Brunauer-Emmett-Teller theory. Meanwhile, the microporous surface area (S_{micro}) was evaluated using the t-plot method (Carbon Black STSA thickness curve). The meso and macro pore surface area ($S_{meso/macro}$) was estimated by the Barrett–Joyner–Halenda (BJH) method. The nitrogen physisorption isotherms are provided in supplementary materials (Figure S7).

2.4.5 Surface morphology using SEM

To assess biochar morphology Scanning Electron Microscopy (SEM) was used. Measurements were done with a TM3000 Tabletop Scanning Electron Microscope (Hitachi, Krefeld, Germany). SEM was performed at an acceleration voltage of 15 kV for all samples. Magnifications were set at 200x and 800x.

2.4.6 Biochar stability using the Edinburgh Stability tool

Biochar stability was determined using a chemical oxidation resistance test (also known as the Edinburgh Stability Tool) as described by Cross et al. [33]. This test corresponds to the stability of biochar in temperate soils during 100 years. Stability was determined by adding 7 ml hydrogen peroxide (5%) solution (diluted from 30% (v/v) H_2O_2, Merck) to a known mass of biochar (corresponding to 0.1 g carbon). Subsequently, the sample was heated to 80 °C and conditioned for 48 h, whereupon the samples were dried at 105 °C. Both residual mass and residual carbon content were measured and biochar stability was calculated using the following formula:

$$Biochar\ stability\ (\%) = \frac{Br \times BrC}{Bt \times BtC}\ x\ 100 \quad (1)$$

With Br, Bt, BrC and BtC corresponding to the residual biochar mass, initial biochar mass, residual biochar carbon content and initial biochar carbon content, respectively.

2.4.7 Biochar aromaticity using ^{13}C – CP/MAS NMR

Carbon-13 solid-state CP/MAS (Cross-Polarization/Magic Angle Spinning) NMR spectra were acquired on a Jeol ECZ 600R 600MHz spectrometer (14.1 T magnet) equipped with a 3.2 mm sHX 32 VT probe. Magic angle spinning was performed at 20 kHz. The aromatic signal of hexamethylbenzene was used to determine the Hartmann-Hahn condition ($\omega_{1H} = \gamma_H B_{1H} = \gamma_C B_{1C} = \omega_{1C}$) for cross-polarization (CP), and to calibrate the carbon chemical shift scale at 132.1 ppm. The following acquisition parameters were applied: a spectral width of 95 kHz, a 90° pulse length of 2.2 μs, a spin-lock field for CP of 85 kHz, a contact time for CP of 1 ms, an acquisition time of 15 ms, a recycle delay time of 2.5 s and about 30000 accumulations. High power proton dipolar decoupling during the acquisition time was set to 80 kHz. The aromatic peak was integrated from around 100 to 145 ppm, the aliphatic peak from around 10 to 50 ppm (Figure S4).

2.4.8 Determination of volatiles in steam distillate by headspace gas chromatography – mass spectroscopy

Headspace (HS) GC-MS analysis was carried out on a Thermo Scientific Trace 1310 system (Waltham, USA) coupled to an ISQ LT Quadrupole MS at a constant helium flow of 1.2 ml/min. The column used was a 30 m length × 0.25 mm internal diameter with a 0.25-µm DB5-MS film capillary column. Samples were measured undiluted, NaCl (30 wt/wt%) was added to improve analyte partitioning before injection. After 30 min headspace at 80 °C, 1 ml was injected in a split mode of 1:10. The injector temperature and the ion source temperature of the detector were 250 and 210 °C. The oven temperature was 30 °C. Then, at 3 min a 10 °C/min ramp, the temperature was raised up to 280 °C, which was maintained for 2 min. Tracked m/z-ratios ranged from 34 – 550.

2.5 Biochar carbon sequestration

The carbon sequestration of biochars can be determined using two distinct biochar properties, carbon retention (i.e. amount of biomass carbon retained in biochar, sometimes referred to as biochar carbon yield [34]) and biochar stability (i.e. amount of the retained carbon sequestered in soil as determined by the Edinburgh stability tool [33]). Hence, the amount of biochar carbon sequesterable in soil was calculated using the following formula:

$$Carbon\ sequestered\ (\%) = BY\ (\%) * \frac{BcC\ (wt\%)}{BmC(wt\%)} * \frac{BS(\%)}{100} \qquad (2)$$

With BY, BcC, BmC and BS corresponding to respectively biochar yields (%), biochar carbon content (wt%), biomass carbon content (wt%) and biochar stability (%).

3 Results and discussion

3.1 Characterization of raw and spent ivy biomass as potential pyrolysis feedstock

First of all, it needs to be assessed whether raw and spent common ivy can be suitable biochar precursors. This depends on the biomass' ultimate analysis, specifically its carbon, nitrogen and ash contents. In view of the biochar's applicability as soil fertilizer, large carbon and nitrogen and moderate ash contents are desirable, as these nutrients are indispensable for plant growth [35]. Furthermore, the ability of the biomass to be converted into porous aromatic carbonaceous materials depends on feedstock properties e.g. the presence and type of lignocellulosic structures (estimated by surface functional groups) and morphology, which influence the carbonization (e.g. biochar yield) and aromatization (e.g. biochar aromaticity) processes, and the formation and escape of volatiles during the pyrolysis process [36].

The ultimate analysis (Table 1) of the ivy biomasses shows that the nitrogen content of RI is quite high (2.33%) compared to other commonly used biomass sources, e.g. barley grass (0.84%) [37], mallee leaf (1.4%) [15] and bamboo (0.27%) [38]. After extraction, this high amount of nitrogen lowers significantly with 14.6% and 48.9% for EI and SI respectively. This is caused by nitrogen being mostly present in the form of amino acids in biomass, with alanine and proline being the most abundant in common ivy [39]. Most of these amino acids are sparingly soluble in ethanol (except for proline 1.5 g/100 g ethanol at room temperature), but moderately soluble in water, which explains the elevated release of nitrogen during steam distillation. At the same time, another nitrogen release mechanism could be the Strecker degradation of α-amino acids (e.g. alanine and proline) to Strecker aldehydes, which would release volatile ammonia as a byproduct during the steam distillation process [40]. This is evidenced by the detection of Strecker aldehydes (2-methylbutanal and 3-methylbutanal) in the steam distillate (Table S1). Lastly, the detection of 2,3-butadione and 2-methylfurane in the steam distillate implies that some Maillard-type

reactions occurred during the steam distillation process which implies that SI's residual nitrogen is fixed in large nitrogen rich structures (melanoidins) [41].

Table 1: Biomass proximate and ultimate analysis (RI: Raw Ivy, EI: Ethanol extracted Ivy, SI: Steam distilled Ivy) (all values are reported on dry basis; $\mu \pm \sigma$, n=3)

Sample	RI	EI	SI
N (wt%)	2.33 ± 0.08	1.99 ± 0.06	1.19 ± 0.02
C (wt%)	45.1 ± 0.2	43.0 ± 0.3	47.7 ± 0.1
H (wt%)	6.21 ± 0.02	6.02 ± 0.08	6.49 ± 0.09
O (wt%)	40.7 ± 0.2	42.6 ± 0.4	40.8 ± 0.2
Ash (wt%)	5.7 ± 0.2	6.4 ± 0.2	3.9 ± 0.1
Volatile matter (wt%)	75.16	75.54	76.3
Fixed carbon (wt%)	18.5	19.38	18.76
Molar O/C	0.678 ± 0.005	0.743 ± 0.009	0.642 ± 0.003
Molar H/C	1.65 ± 0.01	1.68 ± 0.03	1.64 ± 0.02

Carbon contents decreased after ethanol extraction (EI), while the opposite was observed after steam distillation (SI). The decrease in carbon content for EI can be rationalized as ethanol-mainly extracts polar organic compounds, which relatively enhances the amount of ash from 5.7 to 6.4 wt% and subsequently results in a lower carbon content (Table 1). The increase in carbon content for SI can be explained by the dissolution and extraction of inorganic matter from the biomass during the pretreatment, as evidenced by the decreased ash content (Table 1). This extraction occurred due to the condensation of steam on the biomass surface, which can be viewed as a mild hot water extraction. In addition, similar observations have been made for the steam distillation of mallee leaf [15], which confirms the proposed argumentation. For the same solubility-related reasons, ethanol extraction increased the relative total amounts inorganic nutrients in the biomass (comparing EI to RI), which increases the potential of these biomass streams as green fertilizers.

The lignocellulosic composition of the three ivy biomasses was investigated by FTIR analysis (Figure 1). The spectra of lignin, cellulose and hemicellulose can be used as references for

peak assignment, exemplified in supporting materials (Figure S3). The first broad absorption peak at 3365 cm^{-1} (1) can be attributed to –OH stretching vibration, its broad profile demonstrates that it consists of different types of –OH groups (e.g. phenolics, CH_2-OH, …). The normalized peak intensity is lower for EI than for RI, which demonstrates the extraction selectivity of ethanol towards molecules with polar protic functional groups e.g. waxes, oils and fatty acids [22]. Steam distillations also decreased this peak, as –OH functionalities are generally correlated with volatile compounds (e.g. etheric oils), which are identified in HS-GC-MS measurements (Table S1). The small shoulder above 3000 cm^{-1} (2) originates from the C_{sp2}-H stretching vibrations from aromatic compounds, e.g. lignin. The peaks at 2927 cm^{-1} (3) and at 2856 cm^{-1} (4), are assigned to CH_2 asymmetric and symmetric stretching and originate from both lignin and holocellulose. The band at 1738 cm^{-1} (5) can be assigned to the non-conjugated C = O stretching vibration in hemicellulose and lignin. The peak intensity at 1630 cm^{-1} (6) is attributed to the conjugated C = O vibrations in lignin, while the 1514 cm^{-1} (7) signal originates from the aromatic skeletal vibration of lignin. Other bands assigned to lignin are: 1458 cm^{-1} (8) asymmetric C-H deformation in -CH_3, and in-plane scissor vibration of -CH_2- for lignin and carbohydrates, 1230 cm^{-1} (12) syringyl ring and C–O stretch in lignin and xylan and shoulder above 3000 cm^{-1} (2). The largest holocellulose peak that originates from C-C and C-O stretching vibrations at 1020 cm^{-1} (15) is used as normalization reference. Other peaks attributable to holocellulose include 1377 cm^{-1} (10) C-H deformation, 1329 cm^{-1} (11) CH_2 wagging, 1155 cm^{-1} (13) C-O-C β-(1-->4)-glycosidic bond, 1105 cm^{-1} (14) in plane cellulose ring stretch and at 900 cm^{-1} (16) C-H deformation in cellulose. Lastly some absorption bands can be appointed to N-containing compounds (e.g. proteins): the most relevant are the N-H stretch (1), the NH_2-deformation of primary amides (6) and the C-N stretching of secondary amides (11) [42]. The normalized peak intensities of several

absorption bands of SI decrease compared to RI (most pronounced for peak 6). These decreases can be ~~mainly~~ attributed to the extraction of a variety of compounds by the steam distillation condensate, as the FTIR spectrum of the dried steam distillate shows (Figure S2). From the decrease in N-content, it can be inferred that these extracted compounds contain water-soluble proteins (inherently present in common ivy [43]) which have infrared-active functional group vibrations corresponding to the observed decline in peak intensities (6) and (11) in the SI spent biomass residue [42]. These observations suggest that both ethanol extractions and steam distillations do not significantly affect the structural biomass components of RI, as the peaks attributed to the structural cellulose-lignin matrix remain largely unaffected.

Nr.	Wavenumber (cm^{-1})	Functional group	Ref.
1	3365	O–H and N-H stretch	[42], [44]
2	3070	C_{sp2}-H stretching vibration of aromatics (lignin)	[45]
3	2927	CH_2 asymmetric and symmetric stretching	[26]
4	2856		
5	1738	Non-conjugated C═O stretching vibration (hemicellulose, lignin)	[46]
6	1630	Conjugated C=O in lignin	[47]
		NH_2 deformation in primary amides	[42]
7	1514	Aromatic skeletal vibration in lignin	[26]
8	1458	C-H asymmetric deformation in -CH_3, -CH_2- for lignin and carbohydrates	[26]
9	1421	HCH in plane bending vibration	[29]
10	1377	C-H deformation in cellulose and hemicellulose	[29]
11	1329	CH_2 wagging cellulose and hemicellulose	[29]
		C-N stretching secondary amines	[42]
12	1230	syringyl ring and C–O stretch in lignin and xylan	[30]
13	1155	C-O-C holocellulose (beta 1-4 glycosidic bond)	[31]
14	1105	In plane cellulose ring stretch	[31]
15	1020	C-C and C-O stretching vibration in cellulose and hemicellulose	[31]
16	900	C-H deformation in cellulose	[47]

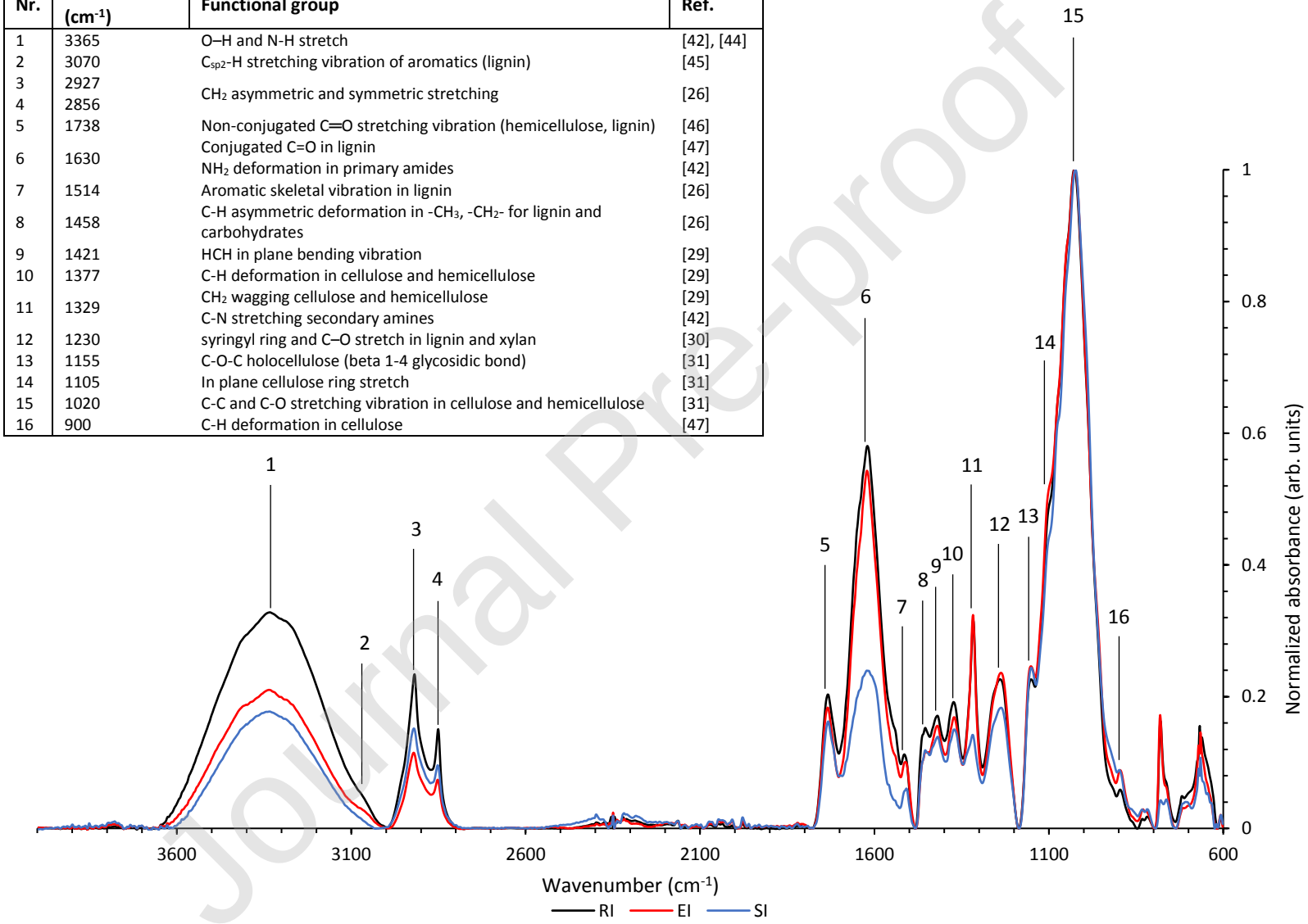

Figure 1: FTIR spectra for biomass (Black: Raw ivy, Red: Ethanol extracted ivy, Blue: Steam distilled ivy)

Steam distillations also influence the microscopic surface of the biomass, as indicated by the SEM-pictures (Figure S5). From a smooth closed surface for RI, a transition towards a more rugged, open structure is observed for SI.

It can be concluded that common ivy and its spent residue are promising candidates for carbonization by slow pyrolysis for further valorization as green fertilizer, thanks to its stable carbon and nutrient content, which will positively impact plant growth as discussed in the first paragraph of this section. Ethanol extractions and steam distillations do not degrade the lignocellulosic structure. Furthermore, SEM-pictures indicate some improvements of the surface morphology of SI compared to RI, hence can be decided to use SI and EI as a feedstock for biochar production.

3.2 Biochar production from common ivy

3.2.1 Influence of pyrolysis temperature on raw ivy biochar properties

Slow pyrolysis of RI at three different pyrolysis temperatures (400, 550 and 700 °C) resulted in three different biochars, RIB-400, RIB-550 and RIB-700. Biochar yields for RIB ranged from 27.6 to 23.0 wt%, inversely proportional to the applied pyrolysis temperature (Table 2). Higher pyrolysis temperatures volatize more organic compounds, as a result of further elimination, cyclisation, condensation and aromatization reactions, which impact the resulting amount of solid residue. These results are in line with comparable studies carried out on different types of agricultural residues (apple tree branches, oak tree, rice husk and rice straw) and bamboo [48–50].

Table 2: Biochar yields, proximate and ultimate analysis of biochars produced at 400, 550 and 700 °C (RIB: Raw Ivy Biochar, EIB: Ethanol extracted Ivy Biochar, SIB: Steam distilled Ivy Biochar) (all values are reported on dry basis; μ ± σ, n=3)

Sample	Yield (wt%)	N (wt%)	C (wt%)	H (wt%)	O (wt%)	Ash (wt%)	Volatile matter (wt%)	Fixed carbon (wt%)	Molar O/C	Molar H/C
RIB-400	27.6 ± 0.9	2.06 ± 0.01	75.0 ± 1.0	2.84 ± 0.06	4 ± 1	16.4 ± 0.3	12.56	72.16	0.04 ± 0.01	0.46 ± 0.01
RIB-550	25.4 ± 0.3	2.07 ± 0.01	70.4 ± 0.6	1.71 ± 0.01	7.2 ± 0.8	18.6 ± 0.5	4.76	69.83	0.077 ± 0.008	0.291 ± 0.003
RIB-700	23.0 ± 0.6	1.81 ± 0.01	74.0 ± 1.0	1.69 ± 0.06	2 ± 1	20.0 ± 0.1	7.24	74.25	0.02 ± 0.01	0.27 ± 0.01
EIB-400	30.6 ± 0.7	2.19 ± 0.05	74.0 ± 1.0	2.55 ± 0.07	4 ± 1	17.1 ± 0.4	9.54	75.42	0.04 ± 0.01	0.41 ± 0.01
EIB-550	28.5 ± 0.7	1.98 ± 0.04	72.3 ± 0.5	1.77 ± 0.04	4.1 ± 0.5	19.8 ± 0.3	13.39	69.48	0.043 ± 0.006	0.293 ± 0.007
EIB-700	25.9 ± 0.5	1.95 ± 0.06	76.3 ± 0.6	1.44 ± 0.06	0.6 ± 0.6	19.7 ± 0.2	10.41	70.34	0.006 ± 0.006	0.227 ± 0.009
SIB-400	25.5 ± 0.5	1.65 ± 0.03	77.1 ± 0.5	2.22 ± 0.06	5.0 ± 0.5	14.0 ± 0.1	13.12	72.23	0.049 ± 0.005	0.35 ± 0.01
SIB-550	23.3 ± 0.1	1.61 ± 0.02	80.5 ± 0.8	1.67 ± 0.03	2.5 ± 0.8	13.7 ± 0.3	7.43	77.8	0.023 ± 0.008	0.248 ± 0.005
SIB-700	21.5 ± 0.7	1.83 ± 0.06	83.2 ± 0.3	1.32 ± 0.04	< 0.5	14.4 ± 0.4	7.59	77.46	< 0.005	0.19 ± 0.01

The pyrolysis process increased the carbon content of all biochars compared to biomass (Table 1 and 2). In addition, fixed carbon and ash content increased by at least 25 and 50% respectively. As such, the resulting biochars are relatively enriched with inorganic nutrients compared to their biomass precursor, as most nutrients do not volatize during the pyrolysis process. For RIB the increase in ash content from 16.4 to 20.0 wt% is proportional with increasing pyrolysis temperatures, in correspondence with preceding studies [15,49].

The RIB's carbon content did not increase proportionally with pyrolysis temperature, which may seem counter-intuitive. However, due to the large ash content of the biochars, a maximal carbon content is already achieved at a lower temperature. With increasing

pyrolysis temperatures, only more carbon, oxygen and hydrogen is released, which increases the ash content but not the carbon content. The stable carbon content also implies that the carbonization process is already well advanced at the lowest pyrolysis temperature, suggesting that 400 °C suffices to produce well-ordered, highly carbonaceous biochars. Only slight decreases in nitrogen content of maximum 0.52 wt% occurred after pyrolysis, indicating a stable incorporation of nitrogen (18 – 35% of initial nitrogen retained) in the biochar structure. Similar values were found by Glarborg et al. [51] for N-retention in wood and straw. All produced biochars are found to comply with the European Biochar Certificate, concerning their O/C and H/C ratio (H/C < 0.7 and O/C < 0.4) [52].

The biochars contain fewer infrared-active diagnostic vibrations, illustrating a general decrease in presence of functional groups (Figure 2). All functionalities in the range of 2700 – 3500 cm^{-1} (-OH) disappeared at pyrolysis temperatures above 400 °C. For RIB at 400 °C, two small peaks are still visible, which correspond to residual aliphatic C-H stretching (I, II). Furthermore, it is demonstrated that the relative intensity of all aromatic bands (650 – 900 cm^{-1}, aromatic C-H out of plane bending (X, XII, XIII)) increase with increasing pyrolysis temperatures. Moreover, from 1000-1300 cm^{-1} (mixture of residual biomass originated moieties [53] (V, VI, VII, VIII)) a large broad plateau can be noted for biochars produced at 400 °C (Figure 2). This plateau gradually shrinks and disappears as a function of pyrolysis temperature, this indicates that the carbonization and aromatization processes are well advanced, but not yet fully completed at 400 °C. This observation is confirmed by the ultimate analysis, where a decrease in H/C ratio occurs with increasing pyrolysis temperatures which indicates an increase in aromaticity (Table 2). These findings are verified by NMR measurements, were the aliphatic carbon peak (30 ppm) decreases with pyrolysis temperature, resulting in spectra with only one broad aromatic peak (125 ppm), which

corresponds to 100% biochar aromaticity (Table 3, Figure S4A). Furthermore, from the FTIR signals at 1400-1450, 875 and 730 cm^{-1} (Figure 2, IV, IX, XII) the presence of carbonates can be demonstrated, which are mostly present as $CaCO_3$ [28].

RIB's display an open surface after pyrolysis (Figure S4), these structures are already observed at 400 °C and retained at higher pyrolysis temperatures of 550 and 700 °C. Moreover, a significant increase in S_{BET} can be noted comparing the RIB produced at 400 and 550 °C with 700 °C (Table 3). This increase is attributed to the creation of micropores (S_{micro}) (accountable for 44.15 m^2/g on a total of 48.57 m^2/g (Table 3)), instigated by the secondary cracking processes of volatile organic matter and the further removal of heteroatoms (O) in the examined temperature range [49]. This volatile organic matter mainly constitutes of lignin and its degradation products as lignin degrades gradually from 150 to 900 °C, while the degradation of cellulose and hemicellulose is already complete at 400 °C [54]. Thus from 550 to 700 °C only further lignin degradation, into various polycyclic aromatic intermediates [49], occurred, leading to product volatilization and opening of pores [55].

It can be concluded that common ivy is a viable feedstock for biochar production. The optimal pyrolysis temperature for biochar fertilizer production is 400 °C: these biochars have a high carbon content and nitrogen content. Also, a high aromaticity is already established at 400 °C, while some residual functional groups are still present. And lastly, biochars produced at this temperature have the highest yields. The earlier described properties would be beneficial for several important properties needed for plant growth, like pH and conductivity, cation exchange capacity and nutrient availability [35]. High carbon and nitrogen contents imply that the amount of ash (i.e. inorganic compounds) is low, which is beneficial for biochar pH and conductivity, as these increase by the leaching of inorganic

material from the biochar's [56]. Also, the degree of aromatization (and presence of surface functional groups) plays a pivotal role in the release of the inorganic nutrients and, as such, in the development of both pH and conductivity [56]. Higher aromaticity enhances the leaching of alkalis and alkaline earth metals from biochars, resulting in enhanced pH and conductivity. Next, the residual (oxygenated) functional groups have a beneficial effect on both the pH (lowers alkalinity) and cation exchange capacity of the biochars [57]. Lastly, nutrient availability is positively correlated with high carbon and nitrogen contents as these are the most important for plant growth, other important nutrients are also removable during the pyrolysis process (e.g. S, P, Cl, K, ..) which indicates that lower pyrolysis temperatures increase the amount of available nutrients [58]. The combination of the three mentioned effects signifies that biochar produced at lower temperatures (400 °C) would be more beneficial for plant growth, compared to high temperature (700 °C) biochars. In addition, this finding has been confirmed (data not shown) in preliminary small-scale plant growth experiments where RIB-400 significantly ($p=0.0003$) improved plant growth compared to a control without biochar addition, while RIB-700 did not show any significant ($p=0.634$) differences with this control.

3.2.2 Effect of extractions on biochar properties

Common ivy was extracted using ethanol or steam distillation, which resulted in a spent ivy biomass. After extraction with ethanol, biochar yields increased significantly for EIB compared to RIB ($p < 0.019$) (Table 2). Which can be explained by the removal of volatile compounds (waxes, fats, chlorophylls, saponins …) by ethanol [22,59], hence the increase in amount of solid residue after pyrolysis. This phenomenon is confirmed by TGA measurements: RI shows a significantly more pronounced decrease in mass below

temperatures of 170 °C, compared to EI (Figure S6A). Conversely, biochar yields were found to decline after steam distillation (Table 2). This can be mainly attributed to the large decrease in ash content, from 16.4 to 14.0 wt%, 18.6 to 13.7 wt% and 20.0 to 14.4 wt% observed when comparing SIBs with RIBs at each of the pyrolysis temperatures (Table 2). This reduction in solid residue is assignable to the condensation of steam on the biomass surface. It can be inferred that parts of the solid minerals dissolved into the liquid phase, as described in section 3.1.

Carbon content increases linearly with pyrolysis temperature for SIB (Table 2). This relation was also found by Gao et al. for the pyrolysis of steam distilled mallee leaf [15]. On the contrary, a slight reduction in carbon content from 400 to 550 °C was found for both RIB (4.6%) and EIB (1.7%). This different behavior of SIB compared with RIB and EIB can be explained by the decreased ash contents of SIB, which allows the carbon contents to increase at higher temperatures (Table 2). After pyrolysis, nitrogen contents of the biochars remained high, ranging from 1.61 – 2.19 wt%, compared with traditional feedstocks with biochar nitrogen contents of 0.34 -0.76 wt% (oak tree [48]) or 0.43 – 0.53 wt% (bamboo [49]). However, SIB's contain up to 20% less nitrogen compared with RIB, due to the release of nitrogen during the pretreatment, as mentioned in section 3.1. These discrepancies in nitrogen content between different pretreatments lowered with increasing pyrolysis temperatures: no significant difference is seen between RIB and SIB at 700 °C ($p = 0.72$). This implies that during the pyrolysis of SI more nitrogen was retained (31 - 35% compared to 18 – 23% for RI). Hence, it can be stated that water-soluble nitrogen species (e.g. amino acids [58]) are already extracted prior to pyrolysis, while the remaining nitrogen species could already be incorporated into larger, stable structures (e.g. melainoidins) by Maillard reactions occurring during steam treatment (section 3.1), hindering the further nitrogen loss

during the subsequent thermal treatment. As such, the nitrogen content originally lost in the steam distillation pre-treatment is compensated by the Maillard reaction induced stable nitrogen incorporation. This finding was previously reported by Xu et al., for the co-pyrolysis of fiberboard with glucose [60], where an increase in glucose increased the extent of occurring Maillard reactions, which then resulted in larger nitrogen retention in the biochars.

SIBs show several distinct differences with RIB and EIB in their FTIR spectra at each pyrolysis temperature (Figure 2). At 400 °C, the peaks in the range of 650 – 850 cm^{-1} (X, XI, XIII) represent the aromatic out of plane C-H bending vibrations, these suggest that SIB has a more aromatic structure compared with RIB. This is also confirmed by the peaks at 2850 and 2950 cm^{-1} (I and II) which correspond to residual aliphatic C-H functionalities, which are still slightly visible for RIB at 400 °C (Figure 2A). The overall decreased absorbance in the 1000 – 1600 cm^{-1} range (bands III, V, VI, VII, VIII)), corresponding to residual biomass functional groups (described in section 3.1), also indicates a higher degree of carbonization for SIB compared with RIB and EIB. This increased carbonization is confirmed by the ^{13}C-NMR spectra (Figure S4B), which proves that SIB is more aromatic (98.22%) than RIB (88.22%) and EIB (94.45%). Also, strong absorption bands corresponding to carbonates (IV, IX, XII) are observed for all samples. The previous confirms that SIB is carbonized and aromatized to a larger extent at 400 °C compared with RIB and EIB.

From 550 °C onward, no bands were observed in the 1800 – 4000 cm^{-1} region, which justifies the x-axis truncation (Figure 2B, C). At 550 °C, the large difference between SIB and RIB/EIB is maintained. The residual biomass functionality signals (1600-1000 cm^{-1}) gradually deflate upon increasing temperature, only peak (VIII) corresponding to a variety of C-O functionalities remains at this pyrolysis temperature. The biochars produced at 700 °C show

the weakest absorption bands corresponding to biochar functional groups. Only the expected aromatic absorption bands (XIII, Figure 2C) are still very pronounced (Table 3). At approximately 1000 cm^{-1} (VIII) some functionalities are seen for RIB and EIB, whereas no signal is observed around this wavenumber for SIB. These signals are assigned to residual C-O functionalities or derive from a mixture of mineral compounds, e.g. P-species (asymmetric stretching vibrations of C-O-P and P-O-P, derived from phosphate, polyphosphate or phosphate esters [61]). The calcium carbonate peaks are also still present at this temperature, although at a lower intensity for SIB, most recognizable from the peak at 875 cm^{-1} (IX). This indicates that the carbonate decomposition, starting at 600 °C [62], is already further advanced for SIB compared to RIB and EIB (Figure 2C). This finding is further supported by the TGA-curves where a lower mass loss is observed for SIB (1.8%) compared with RIB and EIB (respectively 4.8 and 5.5%) in the carbonate degradation temperature interval (Figure S6D).

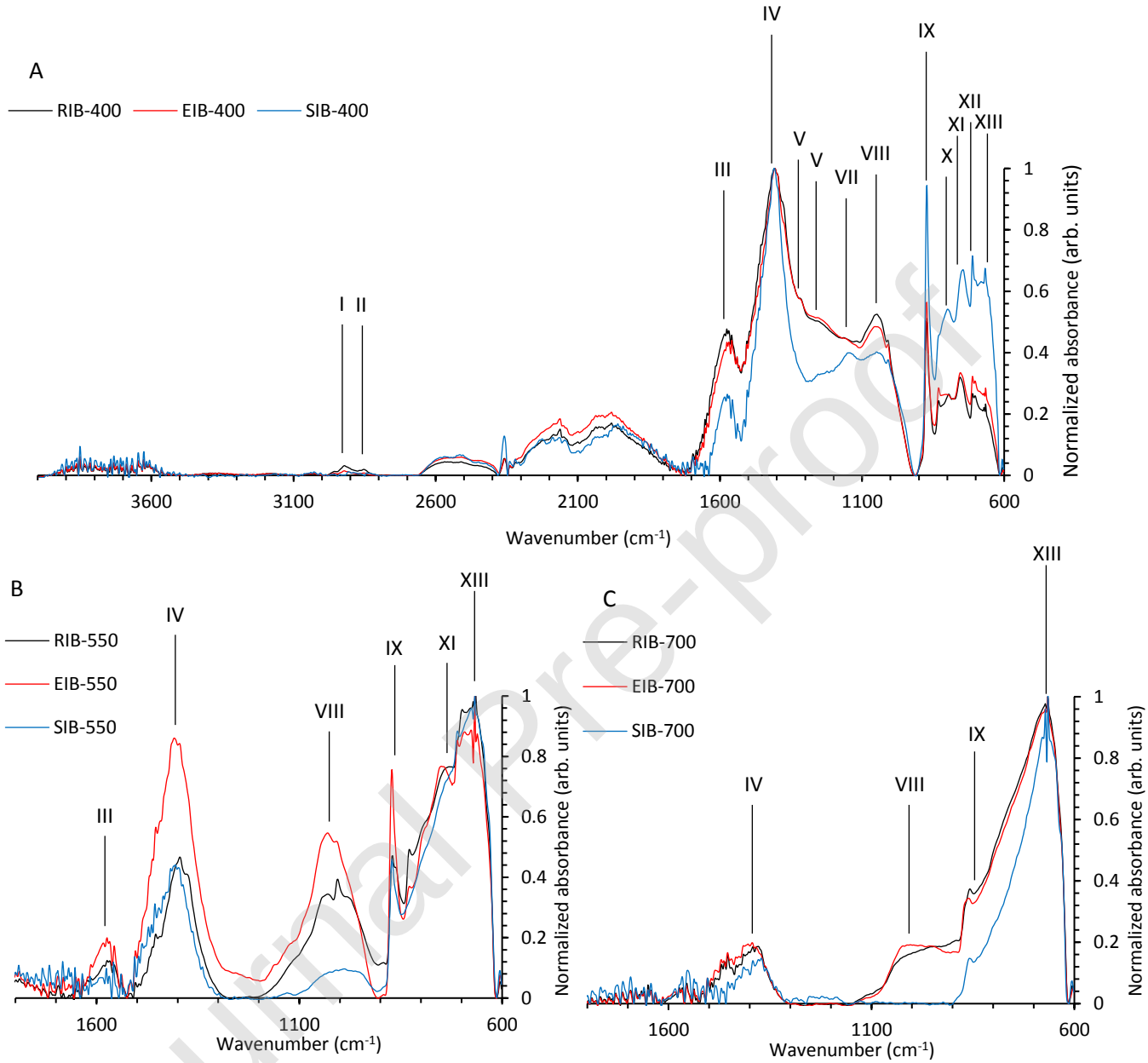

Nr.	Wavenumber (cm^{-1})	Functional group	Ref.
I, II	2950, 2850	Residual aliphatic C-H stretch	[26]
III	1600	Residual C=C from lignin compounds	[27]
IV, IX, XII	1400, 870, 730	$CaCO_3$	[28]
V	1367	Residual CH_2 wagging cellulose and hemicellulose	[29]
VI	1254	Residual syringyl ring and C–O stretch in lignin and xylan	[30]
VII	1150	Residual C-O-C holocellulose (beta 1-4 glycosidic bond)	[31]
VIII	1043	C-O stretching vibration, Mixture of mineral functionalities	[31], [61]
X, XI, XIII	785, 750, 670	Aromatic C-H out of plane bending vibration	[32], [24]

Figure 2: FTIR spectra of biochars (Black: Raw ivy biochar, Red: Ethanol extracted ivy biochar, Blue: Steam distilled ivy biochar)

The S_{BET} RIB and EIB do not exhibit meaningful differences (Table 3), which indicates that comparable carbonization and aromatization processes occurred. This is also supported by previously mentioned results concerning surface functional groups, aromaticity and ultimate analysis. Furthermore, comparable surface structures can be seen when comparing the SEM-images of RI and EI (Figures S4A and S4C). An early increase (550 °C) in S_{BET} manifests itself for SIB's (Table 3), possibly due to the lower amount of ash in these biochars. Two different stages in the pyrolysis process can be distinguished: firstly, a cyclization and aromatization process is observed, where all present carbon is reorganized from its original structure into new polycyclic aromatic carbons. The duration of this stage is dependent on the amount and composition of ash present in the biochar, as the inherent nutrients of the biomass promote a disordered biochar structure [37]. Therefore, a smaller heat requirement is sufficient to recombine the biomass structural components into ordered aromatic compounds. This correlation can be confirmed as the SIB were found to be almost completely aromatized at 400 °C, (Table 3) in contrast to EIB and RIB. The second stage, can be described as a pore formation process (Table 3). In the SIBs, pores already started forming before 550 °C (11.7 m^2/g), while the other samples share a delayed pore formation, which occurs in the 550 - 700 °C temperature range. The created porosity is, just as with the RIB's, attributable to the presence of micropores (S_{micro}) for both SIB and EIB.

Table 3: Biochar functional properties (N/A = not available; μ ± σ, n=3)

Sample	Biochar stability (%)	Aromaticity (%)	S_{BET} (m^2/g)	S_{micro} (m^2/g)	$S_{meso/macro}$ (m^2/g)
RIB-400	88 ± 1	88.22	0.6	N/A	0.5
RIB-550	92 ± 1	100	0.6	N/A	0.4
RIB-700	94 ± 2	100	48.6	44.2	3.3
EIB-400	92 ± 2	94.45	1.3	N/A	0.7
EIB-550	95 ± 2	100	1.6	N/A	0.6
EIB-700	93 ± 1	100	43.4	36.9	4.7
SIB-400	97 ± 1	98.22	1.4	N/A	0.8
SIB-550	95 ± 3	100	11.7	10.3	1.5
SIB-700	97 ± 2	100	40.0	36.1	3.0

The biochar stability estimates the carbon sequestration potential of the produced biochars [33]. The stability of all biochars was very high (>88%, Table 3), which indicates that biochar originating from common ivy is a very viable candidate to be used for soil carbon sequestration. The obtained values were comparable to graphite or mixed wood charcoal as reported by Cross et al. [33]. The biomass' carbonization is already near completion after pyrolysis at all tested pyrolysis temperatures. A proportional relation between biochar stability (88, 92 and 97%) and aromaticity (88, 94 and 98%) can be deduced for the biochars pyrolyzed at 400 °C (Table 3 and Figure S4B). At higher temperatures (550 and 700 °C) all biochar's carbon was aromatic. This was not completely in accordance with the corresponding biochar stabilities, which are between 92 - 97% (Table 3). Some mass loss occurred due to the oxidation of residual oxygen-containing functionalities present in the aromatic structure by H_2O_2, evidenced by the FTIR peak at 1020 cm^{-1} (VIII, Figure 4 b, c). At 700 °C, the biochar stability is identical ($p>0.328$) with 550 °C for all biochars, this corresponds with the identical aromaticity which could be determined by NMR.

Furthermore, it appears that SIB has a higher stability than RIB when both are produced at 400 °C (Table 3). This observation is in line with the previously discussed observations which clearly point out that SIB has fewer C-O/C-N containing surface groups (FTIR) and a higher aromaticity (NMR).

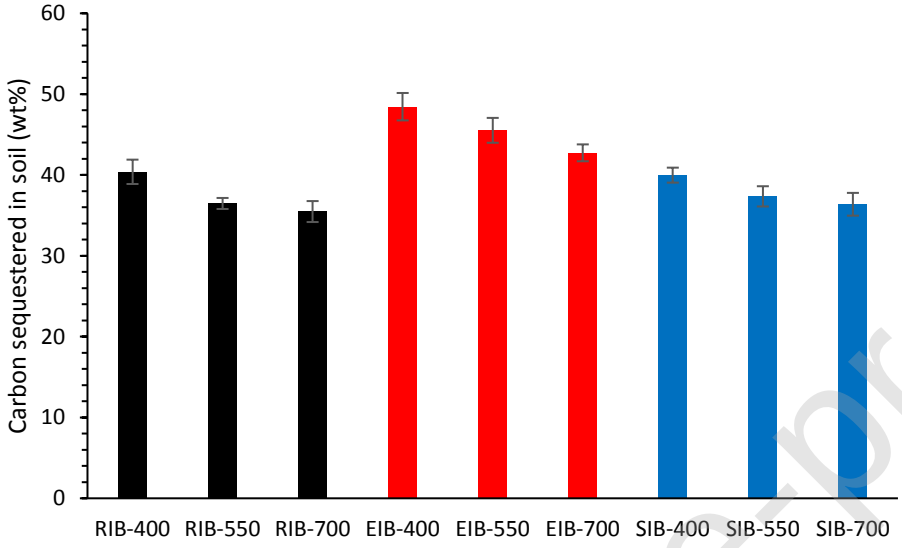

Figure 3: Biochar carbon sequestration potential (Black: Raw ivy biochar, Red: Ethanol extracted ivy biochar, Blue: Steam distilled ivy biochar)

To assess the carbon sequestration potential of the biochars, the amount of carbon released during the pyrolysis process should be taken into account and combined with the biochar stability. This results in the total quantity of carbon sequestered in soil relative to the total carbon present in the biomass. The amount of retained carbon decreases with increasing pyrolysis temperature (Figure 3) from 40 to 36 to 35% with corresponding pyrolysis temperature of 400, 550 and 700 °C, this makes sense, because at higher pyrolysis temperatures more carbon is volatized which results in lower solid carbon residue. Comparing the different pretreatments shows that EIB sequesters more carbon than RIB at each pyrolysis temperature (respectively 48%, 46 and 43% for EIB to 40,36 and 35% for RIB) (Figure 3). This is due to the EIB's having a higher biochar yield at each pyrolysis temperature

(Table 2) and to EI containing less carbon than RI, 43 to 45.1% respectively (Table 1). Both effects signify that the carbon removed by the ethanol extractions (lipids, waxes, saponins etc.) would have been part of the volatized fraction during pyrolysis, as discussed before in section 3.2.1. This makes EI an effective feedstock for carbon sequestration purposes, furthermore the carbon sequestration of 48% from EI-400 is comparable to the 50% proposed by Lehmann et al for biochar soil carbon sequestration [21]. Despite the earlier mentioned increases in biochar stability, steam distillations do not enhance the amount of sequestered carbon, SIB and RIB sequester an equal amount of carbon at each pyrolysis temperature (40, 37 and 36% for SIB's to 39, 36 and 35% for RIB's). This identical carbon sequestration is caused by the increases in biochar stability and carbon contents being balanced by the decreased biochar yields. Both phenomena originate from the dissolution of mineral matter during the steam distillation process which lowers the resulting biochar's ash content, as discussed in section 3.1.

No negative impacts of ethanol extractions on biochar properties can be deduced, on the contrary, positive effects occurred: an increase in biochar yields and biochar stability (when a pyrolysis temperature of 400 °C is applied) lead to an increase in carbon sequestration. Steam distillations display a net positive effect on several biochar properties: biochar yields decreased, carbon contents and biochar stabilities increased. Furthermore, biochars were aromatized at a lower pyrolysis temperature, which is beneficial for the production process as lower temperatures between 400 and 450 °C suffice. In reference to the biochar's applicability as a soil fertilizer, there is no evidence suggesting that the pretreatments would decrease their effectiveness. Moreover, initial small-scale plant growth experiments (data not shown) have indicated that both EIB-400 and SIB-400 improve plant growth similarly as RIB-400 ($p=0.999$ and $p=0.684$, respectively).

Furthermore, this study showed the potential of ivy as feedstock to further develop a scaled process. However, prior to scaling both a techno-economic analysis (TEA) as well as a life-cycle assessment (LCA) on the proposed biorefinery process would be indispensable. A recent TEA provided insight on the viability of an industrial scale slow-pyrolysis plant which converts comparable biomass residue streams into biochar [63]. This study indicated that such a process could be profitable for residue streams with comparable characteristics to common ivy as feedstock. Different independent LCA's demonstrated that pyrolysis-based biorefinery processes significantly reduce GHG-emissions compared to direct biomass combustion [64], biomass combustion coupled with carbon capture and storage [65]. Yang et al. [65] also confirmed the findings of Haledermans et al. [63] that such a process would be profitable. From both analyses, TEA and LCA, can be concluded that our proposed pyrolysis-based biorefinery process with carbon sequestration would be feasible in the near future. However, it should be noted that further research on the impact of upscaling on common ivy biochar properties is still pivotal for the process's large scale application.

4 Conclusions

Common ivy shows great potential as a feedstock for sustainable biorefineries aiming at the valorization of both extractives and spent biomass. It was shown that biochars produced at 400 °C have the most adequate properties to be used as soil fertilizers, due to their high carbon and nitrogen contents, residual surface functionalities and lower ash content. Ethanol extractions had positive effects on biochar yields, ash content and biochar stability which resulted in increased carbon sequestration. Steam distillations lowered the ash content, which led to a higher biochar stability and aromaticity as well as an increase in carbon content compared to RI biochar. However due to steam distillations lowering biochar yields, the amount of sequestered carbon remained identical with RIB. Ultimately all three

biochar streams (RIB, EIB and SIB) would be applicable as green fertilizer while also sequestering significant fractions of carbon in soil. Future research should focus on further elaborating on the biochar's application as a soil fertilizer by performing large-scale plant growth experiments in different types of soil.

Author	Credit
Willem Vercruysse	Conceptualization; Data curation; Funding acquisition; Investigation; Methodology; Project administration; Writing - original draft
Jolien Smeets	Investigation
Tom Haeldermans	Investigation; Writing - review & editing
Bjorn Joos	Investigation; Writing - review & editing
An Hardy	Resources; Writing - review & editing
Pieter Samyn	Resources; Writing - review & editing
Jan Yperman	Resources; Writing - review & editing
Kenny Vanreppelen	Resources; Writing - review & editing
Robert Carleer	Resources; Writing - review & editing
Peter Adriaensens	Resources; Writing - review & editing
Wouter Marchal	Funding Acquisition; Resources; Methodology; Supervision; Writing - review & editing

Dries Vandamme	Funding Acquisition; Methodology; Resources; Supervision; Validation; Writing - review & editing

Declaration of interests

☒ The authors declare that they have no known competing financial interests or personal relationships that could have appeared to influence the work reported in this paper.

4.1 Acknowledgements

This work was financially supported by Research Foundation Flanders (FWO SB – 1S92020N and Hercules project AUHL/15/2 - GOH3816N) and UHasselt BOF (R-10512)). We would like to acknowledge the technicians that have supported and executed the analyses in this study: Gunter Reekmans for the ^{13}C solid state NMR analysis and Martine Vanhamel for FTIR analysis. We would like to acknowledge GGGreen bvba for their valuable input concerning production and valorization of ivy cultured in vertical wall systems.

5 References

[1] T. Sternberg, H. Viles, A. Cathersides, M. Edwards, Dust particulate absorption by ivy (Hedera helix L) on historic walls in urban environments, Sci. Total Environ. 409 (2010) 162–168. https://doi.org/10.1016/j.scitotenv.2010.09.022.

[2] R.W.F. Cameron, J.E. Taylor, M.R. Emmett, What's 'cool' in the world of green façades? How plant choice influences the cooling properties of green walls, Build. Environ. 73 (2014) 198–207. https://doi.org/10.1016/j.buildenv.2013.12.005.

[3] G. Pérez, J. Coma, I. Martorell, L.F. Cabeza, Vertical Greenery Systems (VGS) for energy saving in buildings: A review, Renew. Sustain. Energy Rev. 39 (2014) 139–165. https://doi.org/10.1016/j.rser.2014.07.055.

[4] B. Majester-Savornin, R. Elias, A. Diaz-Lanza, G. Balansard, M. Gasquet, F. Delmas, Saponins of the Ivy Plant, Hedera helix , and their Leishmanicidic Activity, Planta Med. 57 (1991) 260–262. https://doi.org/10.1055/s-2006-960086.

[5] B. Demirci, M. Goppel, F. Demirci, G. Franz, HPLC profiling and quantification of active principles in leaves of Hedera helix L., Pharmazie. 59 (2004) 770–774.

[6] M. Yu, Y.J. Shin, N. Kim, G. Yoo, S.J. Park, S.H. Kim, Determination of Saponins and Flavonoids in Ivy leaf extracts using HPLC-DAD, J. Chromatogr. Sci. 53 (2015) 478–483. https://doi.org/10.1093/chromsci/bmu068.

[7] Y. Lutsenko, W. Bylka, I. Matławska, R. Darmohray, Hedera helix as a medicinal plant, Herba Pol. 56 (2010) 84–96.

[8] European Medicines Agency, Hedera helicis folium - AR, 2018. www.ema.europa.eu/contact.

[9] A.E. Al-snafi, Pharmacological and therapeutic activities of Hedera helix-A review, IOSR J. Pharm. 8 (2018) 41–53.

[10] Y. Gaillard, P. Blaise, A. Darré, T. Barbier, G. Pépin, An unusual case of death: Suffocation caused by leaves of common ivy (Hedera helix). Detection of hederacoside C, α-hederin, and hederagenin by LC-EI/MS, J. Anal. Toxicol. 27 (2003) 257–262. https://doi.org/10.1093/jat/27.4.257.

[11] O. Roşca-Casian, C. Mircea, L. Vlase, A.M. Gheldiu, D.T. Teuca, M. Pârvu, Chemical composition and antifungal activity of Hedera helix leaf ethanolic extract, Acta Biol. Hung. 68 (2017) 196–207. https://doi.org/10.1556/018.68.2017.2.7.

[12] F. Runkel, W. Schneider, O. Schmidt, G.M. Engelhard, Process for preparing an extract from ivy leaves, US 7,943,184 B2, 2011. https://doi.org/10.1038/incomms1464.

[13] A.O. Tucker, M.J. Maciarello, Essential Oil of English Ivy, *Hedera helix* L. 'Hibernica,' J. Essent. Oil Res. 6 (1994) 187–188. https://doi.org/10.1080/10412905.1994.9698352.

[14] S. Yani, X. Gao, P. Grayling, H. Wu, Steam distillation of mallee leaf: Extraction of 1,8-cineole and changes in the fuel properties of spent biomass, Fuel. 133 (2014) 341–349. https://doi.org/10.1016/j.fuel.2014.05.030.

[15] X. Gao, S. Yani, H. Wu, Pyrolysis of spent biomass from mallee leaf steam distillation: Biochar properties and recycling of inherent inorganic nutrients, Energy and Fuels. 28 (2014) 4642–4649. https://doi.org/10.1021/ef501114v.

[16] V. Dhyani, T. Bhaskar, A comprehensive review on the pyrolysis of lignocellulosic biomass, Renew. Energy. 129 (2018) 695–716. https://doi.org/10.1016/j.renene.2017.04.035.

[17] Y.S. Ok, S.X. Chang, B. Gao, H.-J. Chung, SMART biochar technology—A shifting paradigm towards advanced materials and healthcare research, Environ. Technol. Innov. 4 (2015) 206–209. https://doi.org/10.1016/j.eti.2015.08.003.

[18] A. El-Naggar, A.H. El-Naggar, S.M. Shaheen, B. Sarkar, S.X. Chang, D.C.W. Tsang, J. Rinklebe, Y.S. Ok, Biochar composition-dependent impacts on soil nutrient release, carbon mineralization, and potential environmental risk: A review, J. Environ. Manage. 241 (2019) 458–467. https://doi.org/10.1016/j.jenvman.2019.02.044.

[19] M. Marmiroli, U. Bonas, D. Imperiale, G. Lencioni, F. Mussi, N. Marmiroli, E. Maestri, Structural and functional features of chars from different biomasses as potential plant amendments, Front. Plant Sci. 9 (2018) 1–13. https://doi.org/10.3389/fpls.2018.01119.

[20] C. Santín, S.H. Doerr, A. Merino, T.D. Bucheli, R. Bryant, P. Ascough, X. Gao, C.A. Masiello, Carbon sequestration potential and physicochemical properties differ between wildfire charcoals and slow-pyrolysis biochars, Sci. Rep. 7 (2017) 1–11. https://doi.org/10.1038/s41598-017-10455-2.

[21] J. Lehmann, J. Gaunt, M. Rondon, Bio-char Sequestration in Terrestrial Ecosystems – A Review, Mitig. Adapt. Strateg. Glob. Chang. 11 (2006) 403–427. https://doi.org/10.1007/s11027-005-9006-5.

[22] ASTM International, Standard Test Method for Determination of Ethanol Extractives in Biomass, ASTM Stand. 11 (2004) 1–2.

[23] K. Vanreppelen, S. Vanderheyden, T. Kuppens, S. Schreurs, J. Yperman, R. Carleer, Activated carbon from pyrolysis of brewer's spent grain: Production and adsorption properties, Waste Manag. Res. (2014). https://doi.org/10.1177/0734242X14538306.

[24] T. Haeldermans, J. Claesen, J. Maggen, R. Carleer, J. Yperman, P. Adriaensens, P. Samyn, D. Vandamme, A. Cuypers, K. Vanreppelen, S. Schreurs, Microwave assisted and conventional pyrolysis of MDF – Characterization of the produced biochars, J. Anal. Appl. Pyrolysis. 138 (2019) 218–230. https://doi.org/10.1016/j.jaap.2018.12.027.

[25] ASTM International, Standard Test Method for Total Ash Content of Activated Carbon, ASTM Stand. 15 (2004) 1–2. https://doi.org/10.1520/D2866-11.2.

[26] O. Faix, Classification of Lignins from Different Botanical Origins by FT-IR Spectroscopy, Holzforschung. 45 (1991) 21–28. https://doi.org/10.1515/hfsg.1991.45.s1.21.

[27] C.H. Chia, B. Gong, S.D. Joseph, C.E. Marjo, P. Munroe, A.M. Rich, Imaging of mineral-enriched

biochar by FTIR, Raman and SEM-EDX, Vib. Spectrosc. 62 (2012) 248–257. https://doi.org/10.1016/j.vibspec.2012.06.006.

[28] B. Singh, M. Camps-Arbestain, J. Lehmann, CSIRO (Australia), Biochar: A Guide to Analytical Methods, 2017. https://books.google.co.uk/books?hl=en&lr=&id=ieRrDgAAQBAJ&oi=fnd&pg=PP1&dq=biochar:+a+guide+to+analytical+methods&ots=zBBO1rVDD7&sig=ysnb7inmaSDYu1EHCJSbOkejehg&redir_esc=y#v=onepage&q&f=false.

[29] C.Y. Liang, R.H. Marchessault, Infrared spectra of crystalline polysaccharides. II. Native celluloses in the region from 640 to 1700 cm.1, J. Polym. Sci. 39 (1959) 269–278. https://doi.org/10.1002/pol.1959.1203913521.

[30] G. Müller, C. Schöpper, H. Vos, A. Kharazipour, A. Polle, FTIR-ATR spectroscopic analyses of changes in wood properties during particleand fibreboard production of hardand softwood trees, BioResources. 4 (2009) 49–71. https://doi.org/10.15376/biores.4.1.49-71.

[31] A.M. Raspolli Galletti, A. D'Alessio, D. Licursi, C. Antonetti, G. Valentini, A. Galia, N. Nassi O Di Nasso, Midinfrared FT-IR as a tool for monitoring herbaceous biomass composition and its conversion to furfural, J. Spectrosc. 2015 (2015). https://doi.org/10.1155/2015/719042.

[32] Y. Liu, Z. He, M. Uchimiya, Comparison of Biochar Formation from Various Agricultural By-Products Using FTIR Spectroscopy, Mod. Appl. Sci. 9 (2015) 246–253. https://doi.org/10.5539/mas.v9n4p246.

[33] A. Cross, S.P. Sohi, A method for screening the relative long-term stability of biochar, GCB Bioenergy. 5 (2013) 215–220. https://doi.org/10.1111/gcbb.12035.

[34] M.J. Antal, M. Grønli, The Art, Science, and Technology of Charcoal Production, Ind. Eng. Chem. Res. 42 (2003) 1619–1640. https://doi.org/10.1021/ie0207919.

[35] A.K. Patel, Land Applications of Biochar: An Emerging Area, in: Waste to Wealth, Energy, Environ. Sustain., 2018: pp. 171–197. https://doi.org/10.1007/978-981-10-7431-8_9.

[36] T. Kan, V. Strezov, T.J. Evans, Lignocellulosic biomass pyrolysis: A review of product properties and effects of pyrolysis parameters, Renew. Sustain. Energy Rev. 57 (2016) 1126–1140. https://doi.org/10.1016/j.rser.2015.12.185.

[37] H. Nan, F. Yang, L. Zhao, O. Mašek, X. Cao, Z. Xiao, Interaction of Inherent Minerals with Carbon during Biomass Pyrolysis Weakens Biochar Carbon Sequestration Potential, ACS Sustain. Chem. Eng. 7 (2019) 1591–1599. https://doi.org/10.1021/acssuschemeng.8b05364.

[38] W. Chen, Y. Chen, H. Yang, M. Xia, K. Li, X. Chen, H. Chen, Co-pyrolysis of lignocellulosic biomass and microalgae: Products characteristics and interaction effect, Bioresour. Technol. 245 (2017) 860–868. https://doi.org/10.1016/j.biortech.2017.09.022.

[39] I. Bezruk, M. Marksa, V. Georgiyants, L. Ivanauskas, L. Raudone, Phytogeographical profiling of ivy leaf (Hedera helix L.), Ind. Crops Prod. 154 (2020) 112713. https://doi.org/10.1016/j.indcrop.2020.112713.

[40] D. Rainer Cremer, K. Eichner, The reaction kinetics for the formation of Strecker aldehydes in low moisture model systems and in plant powders, Food Chem. 71 (2000) 37–43. https://doi.org/10.1016/S0308-8146(00)00122-9.

[41] Z. Wang, Strecker Degradation, Compr. Org. Name React. Reagents. (2010) 2701–2706. https://doi.org/10.1002/9780470638859.conrr607.

[42] G. Bekiaris, G. Koutrotsios, P.A. Tarantilis, C.S. Pappas, G.I. Zervakis, FTIR assessment of

compositional changes in lignocellulosic wastes during cultivation of Cyclocybe cylindracea mushrooms and use of chemometric models to predict production performance, J. Mater. Cycles Waste Manag. 22 (2020) 1027–1035. https://doi.org/10.1007/s10163-020-00995-7.

[43] L. Ferrara, D. Naviglio, S. Faralli, Identification of Active Principles of Hedera helix L. in aqueous extracts, in: J. Phytochem. Phot., 2013: pp. 170–175. https://www.researchgate.net/profile/Daniele_Naviglio/publication/236329898_Identification_of_Active_Principles_of_Hedera_helix_L_in_aqueous_extracts/links/0deec517a295a7f622000000/Identification-of-Active-Principles-of-Hedera-helix-L-in-aqueous-extracts.

[44] K.K. Pandey, A.J. Pitman, FTIR studies of the changes in wood chemistry following decay by brown-rot and white-rot fungi, Int. Biodeterior. Biodegrad. 52 (2003) 151–160. https://doi.org/10.1016/S0964-8305(03)00052-0.

[45] K.K. Dasari, V. Gumtapure, S. Dutta, Upgrading of coconut shell-derived pyrolytic bio-oil by thermal and catalytic deoxygenation, Energy Sources, Part A Recover. Util. Environ. Eff. 00 (2020) 1–10. https://doi.org/10.1080/15567036.2019.1711465.

[46] M.M. Rahman, A.K. Mallik, M.A. Khan, Influences of various surface pretreatments on the mechanical and degradable properties of photografted oil palm fibers, J. Appl. Polym. Sci. 105 (2007) 3077–3086. https://doi.org/10.1002/app.26481.

[47] X. Wang, H. Ren, Comparative study of the photo-discoloration of moso bamboo (Phyllostachys pubescens Mazel) and two wood species, Appl. Surf. Sci. 254 (2008) 7029–7034. https://doi.org/10.1016/j.apsusc.2008.05.121.

[48] K. Jindo, H. Mizumoto, Y. Sawada, M.A. Sanchez-Monedero, T. Sonoki, Physical and chemical characterization of biochars derived from different agricultural residues, Biogeosciences. 11 (2014) 6613–6621. https://doi.org/10.5194/bg-11-6613-2014.

[49] H. Wang, X. Wang, Y. Cui, Z. Xue, Y. Ba, Slow pyrolysis polygeneration of bamboo (Phyllostachys pubescens): Product yield prediction and biochar formation mechanism, Bioresour. Technol. 263 (2018) 444–449. https://doi.org/10.1016/j.biortech.2018.05.040.

[50] D. Chen, J. Zhou, Q. Zhang, Effects of heating rate on slow pyrolysis behavior, kinetic parameters and products properties of moso bamboo, Bioresour. Technol. 169 (2014) 313–319. https://doi.org/10.1016/j.biortech.2014.07.009.

[51] P. Glarborg, Fuel nitrogen conversion in solid fuel fired systems, Prog. Energy Combust. Sci. 29 (2003) 89–113. https://doi.org/10.1016/S0360-1285(02)00031-X.

[52] EBC (2012), European Biochar Certificate - Guidelines for a Sustainable Production of Biochar', Eur. Biochar Found. (EBC), Arbaz, Switzerland. Version 6.1 19th June,. (2020) 1–22. https://doi.org/10.13140/RG.2.1.4658.7043.

[53] L. Huang, Y. Chen, G. Liu, S. Li, Y. Liu, X. Gao, Non-isothermal pyrolysis characteristics of giant reed (Arundo donax L.) using thermogravimetric analysis, Energy. 87 (2015) 31–40. https://doi.org/10.1016/j.energy.2015.04.089.

[54] H. Yang, R. Yan, H. Chen, D.H. Lee, C. Zheng, Characteristics of hemicellulose, cellulose and lignin pyrolysis, Fuel. 86 (2007) 1781–1788. https://doi.org/10.1016/j.fuel.2006.12.013.

[55] J.W.C. Wong, J.B.W. Webber, U.O. Ogbonnaya, Characteristics of biochar porosity by NMR and study of ammonium ion adsorption, J. Anal. Appl. Pyrolysis. 143 (2019) 104687. https://doi.org/10.1016/j.jaap.2019.104687.

[56] J. Sun, F. He, Y. Pan, Z. Zhang, Effects of pyrolysis temperature and residence time on

physicochemical properties of different biochar types, Acta Agric. Scand. Sect. B — Soil Plant Sci. 67 (2017) 12–22. https://doi.org/10.1080/09064710.2016.1214745.

[57] R.R. Domingues, M.A. Sánchez-Monedero, K.A. Spokas, L.C.A. Melo, P.F. Trugilho, M.N. Valenciano, C.A. Silva, Enhancing Cation Exchange Capacity of Weathered Soils Using Biochar: Feedstock, Pyrolysis Conditions and Addition Rate, Agronomy. 10 (2020) 824. https://doi.org/10.3390/agronomy10060824.

[58] W.J. Liu, W.W. Li, H. Jiang, H.Q. Yu, Fates of Chemical Elements in Biomass during Its Pyrolysis, Chem. Rev. 117 (2017) 6367–6398. https://doi.org/10.1021/acs.chemrev.6b00647.

[59] M. Ishiwatari, R. Ishiwatari, H. Sakashita, T. Tatsumi, Thermogravimetry and pyrolysis-GC of chlorophyll-a: with a special emphasis on thermal behavior of its phytyl chain, J. Anal. Appl. Pyrolysis. 35 (1995) 237–247. https://doi.org/10.1016/0165-2370(95)00914-4.

[60] D. Xu, L. Yang, M. Zhao, Y. Song, Karnowo, H. Zhang, X. Hu, H. Sun, S. Zhang, N evolution and physiochemical structure changes in chars during co-pyrolysis: Effects of abundance of glucose in fiberboard, Energies. 13 (2020). https://doi.org/10.3390/en13195105.

[61] Q. Zhou, X. Jiang, X. Li, C.Q. Jia, W. Jiang, Preparation of high-yield N-doped biochar from nitrogen-containing phosphate and its effective adsorption for toluene, RSC Adv. 8 (2018) 30171–30179. https://doi.org/10.1039/c8ra05714a.

[62] E.E. Kwon, T. Lee, Y.S. Ok, D.C.W. Tsang, C. Park, J. Lee, Effects of calcium carbonate on pyrolysis of sewage sludge, Energy. 153 (2018) 726–731. https://doi.org/10.1016/j.energy.2018.04.100.

[63] T. Haeldermans, L. Campion, T. Kuppens, K. Vanreppelen, A. Cuypers, S. Schreurs, A comparative techno-economic assessment of biochar production from different residue streams using conventional and microwave pyrolysis, Bioresour. Technol. 318 (2020) 124083. https://doi.org/10.1016/j.biortech.2020.124083.

[64] J.F. Peters, D. Iribarren, J. Dufour, Biomass Pyrolysis for Biochar or Energy Applications? A Life Cycle Assessment, Environ. Sci. Technol. 49 (2015) 5195–5202. https://doi.org/10.1021/es5060786.

[65] Q. Yang, H. Zhou, P. Bartocci, F. Fantozzi, O. Mašek, F.A. Agblevor, Z. Wei, H. Yang, H. Chen, X. Lu, G. Chen, C. Zheng, C.P. Nielsen, M.B. McElroy, Prospective contributions of biomass pyrolysis to China's 2050 carbon reduction and renewable energy goals, Nat. Commun. 12 (2021) 1698. https://doi.org/10.1038/s41467-021-21868-z.